HIGH-FIDELITY EXPERIMENTAL MODEL VERIFICATION FOR FLOW IN FRACTURED POROUS MEDIA

Jakub Wiktor Both[1] (iD), Bergit Brattekås[2] (iD), Eirik Keilegavlen[1] (iD), Martin A. Fernø[2,3] (iD), Jan Martin Nordbotten[1,3] (iD)

[1]Centre for Modeling of Coupled Subsurface Dynamics, Department of Mathematics, University of Bergen, Bergen, Norway; [2]Department of Physics and Technology, University of Bergen, Bergen, Norway; [3]Norwegian Research Center, NORCE, Bergen, Norway

A   ADDITIONAL SNAPSHOTS SUBSTANTIATING THE MODEL VERIFICATION

Side-by-side comparisons serve as a key method in the main text for evaluating the quality of the match between the model and experiments. As in the aforementioned qualitative analysis, three snapshots from each fluid displacement experiment are provided to visually compare plume shapes across experiments, complemented by Wasserstein flux illustrations to indicate match quality. Auxiliary close-up views of marked regions highlight the most visually pronounced discrepancies. The development of the fronts for Cores A, A*, B, and C is displayed in **Figure 1S**, **Figure 2S**, **Figure 3S**, and **Figure 4S**, respectively. The additional snapshots substantiate the observations and analysis of the main material.

The visual material is further supported by illustrations of Wasserstein fluxes, providing a visual representation of the Wasserstein distance discussed in Section B. **Figure 5S** offers a closer look at several Wasserstein fluxes, corresponding to the same time steps as referenced above. In addition, the experimental and numerical 3D data are overlaid to demonstrate a close fit in terms of shape. Supplementing **Figure 4** in the main text, **Figure 6S** provides close-up views of Wasserstein flux snapshots, highlighting the optimal transport distance between Core A and Core A*.
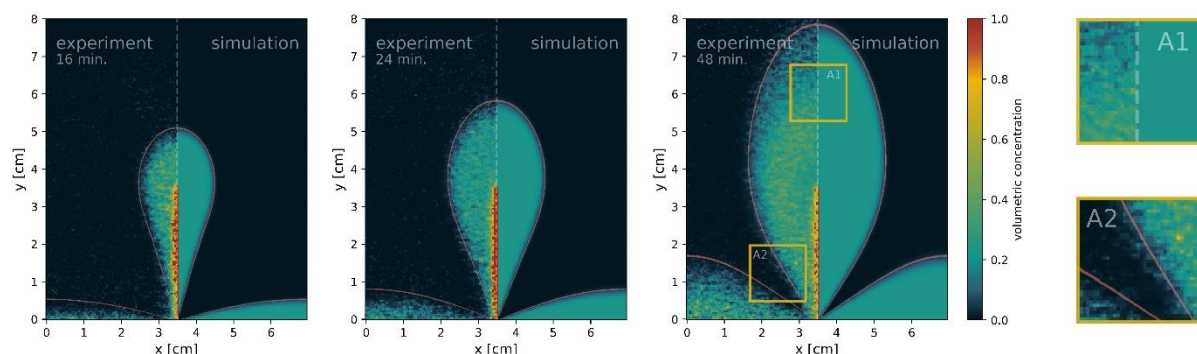

Figure 1S: Core A: Evolution of the (essentially symmetric) tracer concentration plumes for the experimental results, presented in side-by-side comparison with the corresponding numerical simulation. An additional 5% contour line is included to aid visual comparison. Close-up visualizations highlight two characteristic regions with dispersive undershoots and overshoots.
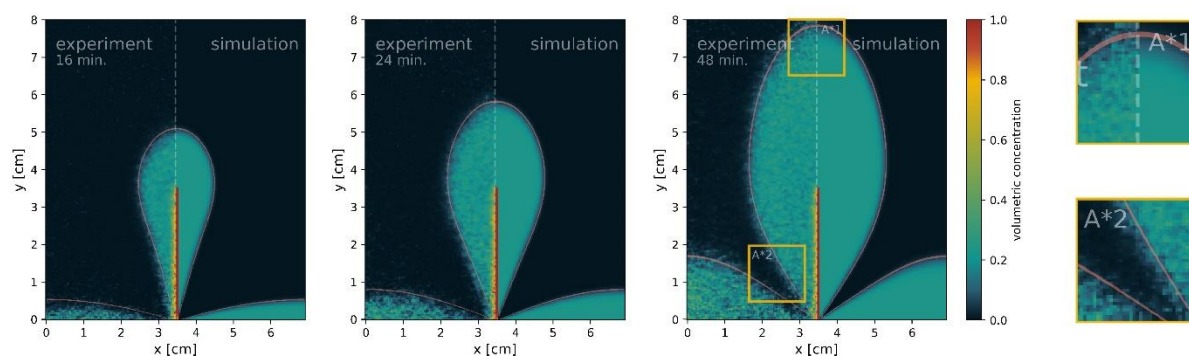
Figure 2S: Core A*: Evolution of the (essentially symmetric) tracer concentration plumes for the experimental results, presented in side-by-side comparison with the corresponding numerical simulation. An additional 5% contour line is included to aid visual comparison. Close-up visualizations highlight two characteristic regions with dispersive undershoots and overshoots.
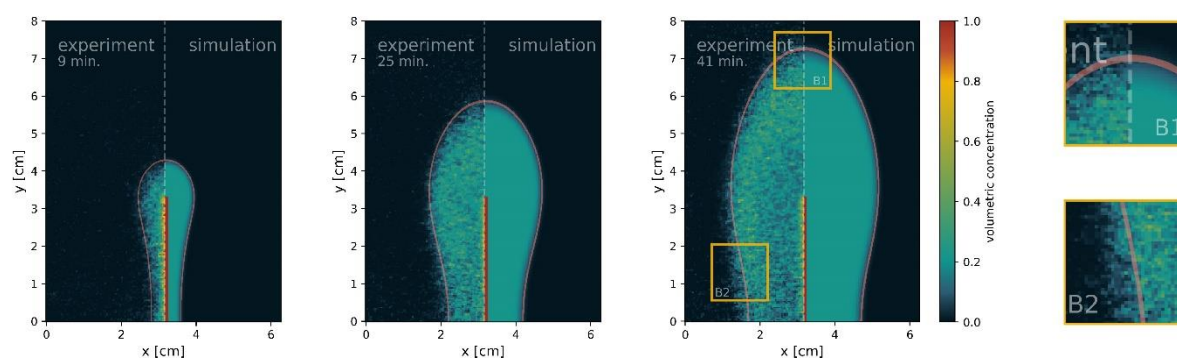

Figure 3S: Core B: Evolution of the (essentially symmetric) tracer concentration plumes for the experimental results, presented in side-by-side comparison with the corresponding numerical simulation. An additional 5% contour line is included to aid visual comparison. Close-up visualizations highlight two characteristic regions with dispersive undershoots and overshoots.

Figure 4S: Core C: Evolution of the (essentially symmetric) tracer concentration plumes for the experimental results, presented in side-by-side comparison with the corresponding numerical simulation. An additional 5% contour line is included to aid visual comparison. Close-up visualizations highlight two characteristic regions with dispersive undershoots and overshoots.
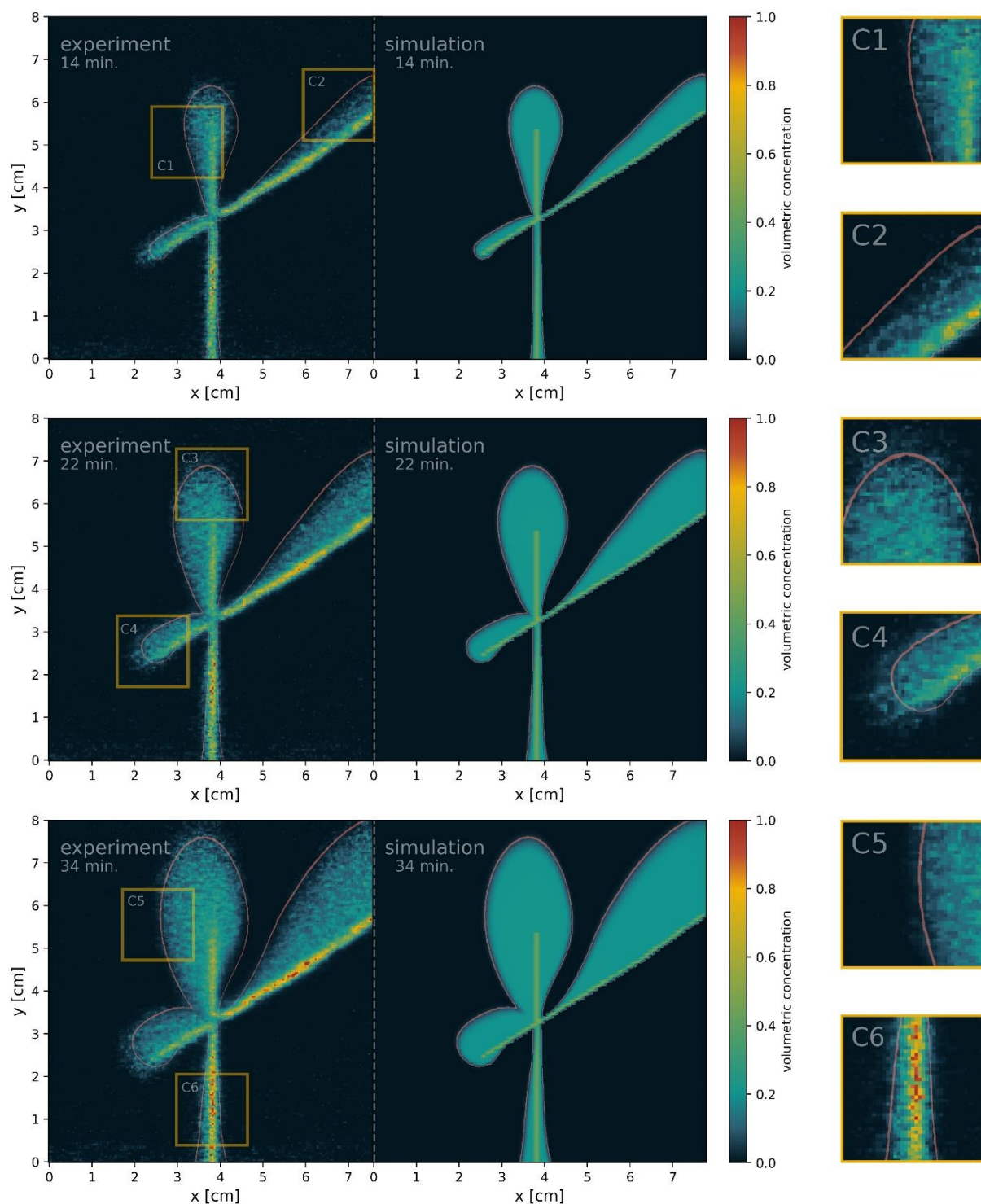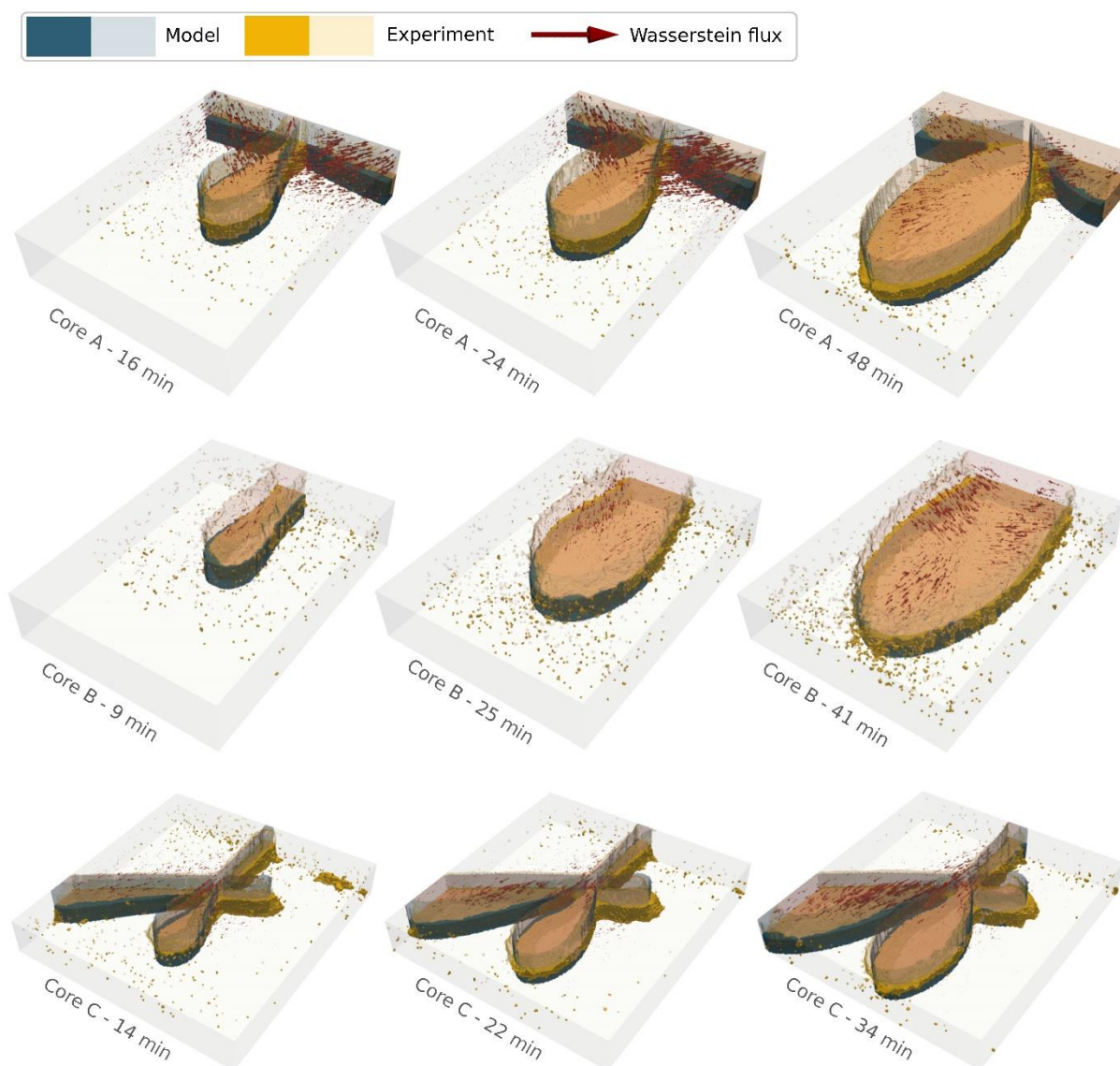
Figure 5S: Cores A, B, C: Three-dimensional qualitative comparison of tracer plumes corresponding to **Figures 1S**, **3S**, and **4S**. The upper and lower plumes are displayed transparently. Additionally, scaled Wasserstein fluxes are shown to illustrate the conversion from one distribution to another.
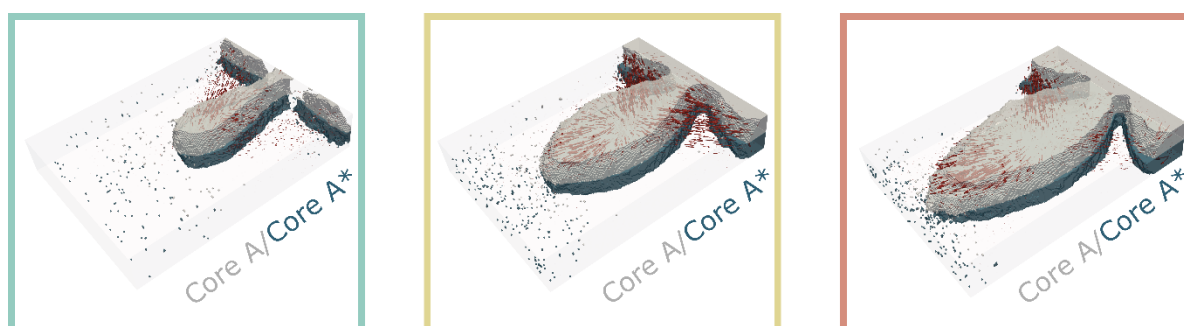

Figure 6S: Cores A/A*: Scaled Wasserstein fluxes are displayed to illustrate the conversion from one distribution to the other, corresponding to **Figure 4** in main text.

B   WASSERSTEIN METRIC ENTERING THE QUANTITATIVE ANALYSIS AND ERROR QUANTITIES

The quantitative analysis in the main text relies extensively on the Wasserstein distance, as summarized below. Additionally, a statistical analysis of regularization and experimental errors is conducted to confirm the high quality of the study's experimental data.

B.1   Relative Wasserstein distance

The quantitative analysis presented in the main text is based on the Wasserstein distance measuring the difference between upscaled laboratory data and simulation data. We recall a standard definition of the 1-Wasserstein distance in terms of the solution of a variational problem also called Beckmann problem (2). For two compatible concentration profiles, c_A and c_B, defined over the domain Ω with $\int_\Omega c_A dx = \int_\Omega c_B dx$, we define the 1-Wasserstein distance to be (**Eq. S1**):

$$W^1\,c_A, c_B = \inf\left\{\int_\Omega |q|\,dx : \nabla \cdot q = c_A - c_B \text{ in } \Omega\right\} \tag{S1}$$

The associated flux q is also termed *Wasserstein flux* in the main material. To compute $W^1\,c_A, c_B$ for voxel distributions c_A and c_B, we use a numerical approximation (1). To put the results of the quantitative analysis in context, relative distances have been used. Using the average transport distance as the reference value, we consider the relative distance between two concentration profiles, c_A (typically experimental data) and c_B (typically simulation data) (**Eq. S2**):

$$\text{Relative Wasserstein distance} = \frac{W^1\,c_A, c_B}{W^1(c_A, \delta_{c_A, \Gamma})} \tag{S2}$$

where $\delta_{c_A, \Gamma}$ denotes a Dirac-type concentration variant of c_A with same total mass but concentrated to some part of the domain Γ; i.e., $\delta_{c_A, \Gamma}$ has support in Γ, is constant on Γ and satisfies $\int_\Omega \delta_{c_A, \Gamma} dx = \int_\Omega c_A dx$. Here, we choose Γ to be the intersection of the inlet and the connected fracture, cf. **Figure 7S**. By design the relative Wasserstein distance is unit-free. Values of the order 1 indicate a first-order deviation from the reference data (here c_A).
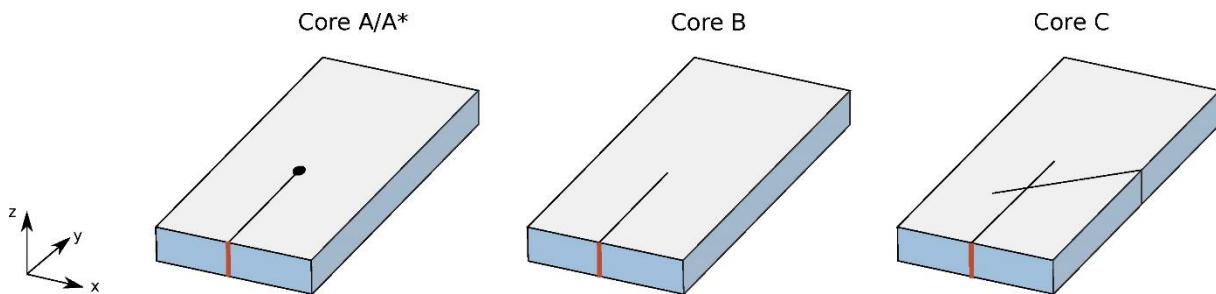

Figure 7S: Support $\boldsymbol{\Gamma}$ for Dirac variants of Cores A/A*B, and C, indicated in red. Refer to **Figure 3** in the main text for complete geometrical specifications.

B.2   Regularization error

The upscaled data is obtained through regularization of the raw, to large extent sparse, and noisy PET signal. As the used regularization (total variation denoising) enables inpainting, the Wasserstein distance between the raw and regularized signals, rescaled to same mass, identifies the cost required to distribute the sparse signal. This distribution is of local nature and thus identifies a small reference distance. The regularization error given by the Wasserstein distance between raw and regularized data for the four experiments (Cores A, A*, B, and C) are displayed in **Figure 8Sa**; we employ relative distances with the reference value defined through the regularized data, compatible with the quantitative analysis in the main material. We conclude that the relative regularization error is approximately 0.05 ± 0.03, indicating that the regularization error is relatively low.
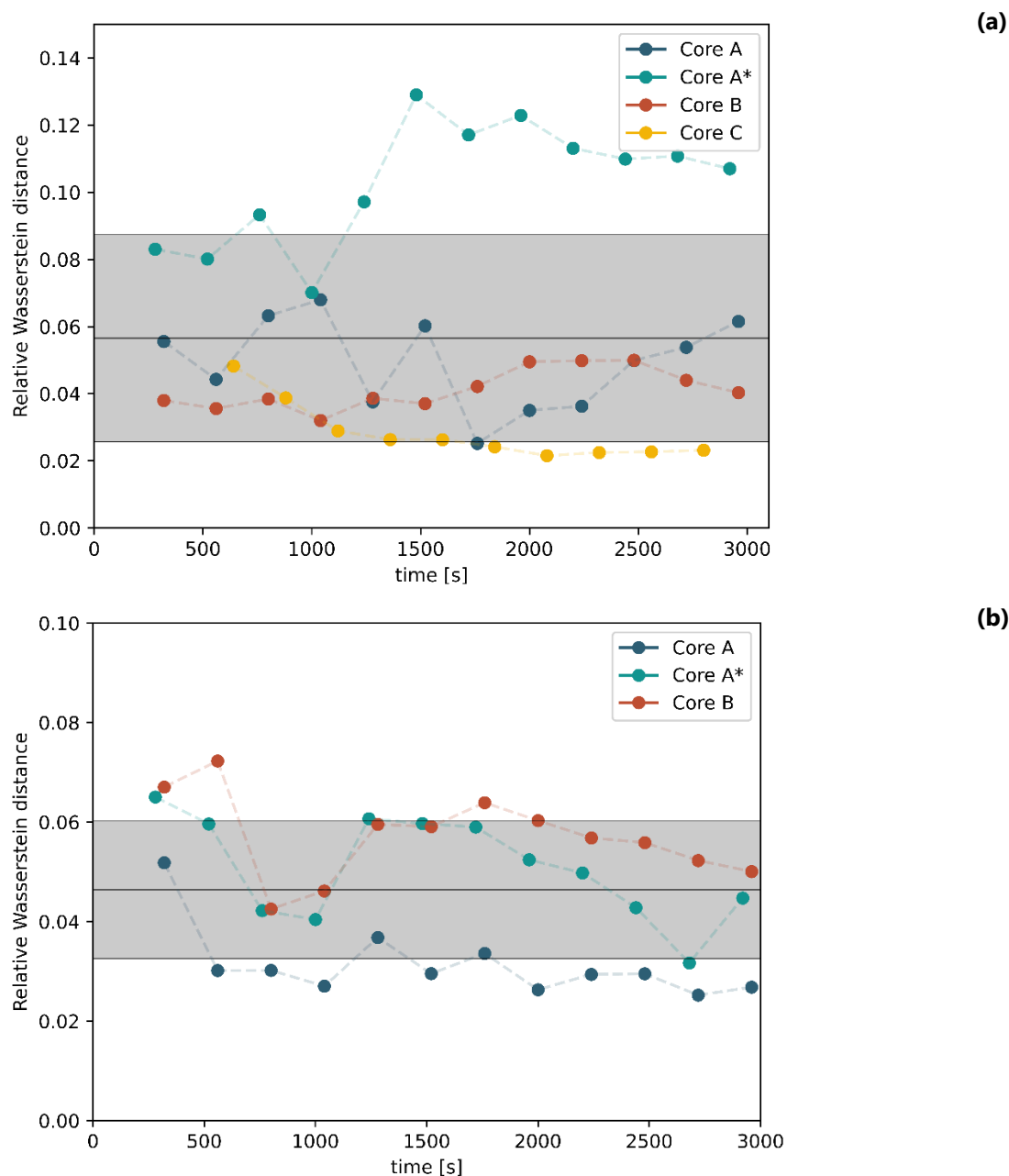
Figure 8S: Relative regularization and symmetry error for all experiments across all time steps, with the mean and standard deviation illustrated by a gray box.

B.3   Experimental variability measure

The experiments for Cores A, A*, and B are designed to be plane symmetric. However, imperfections in the experiments arising from nearly isotropic conditions and various influences (e.g., operating conditions) naturally affect fluid displacement. Ultimately, the resulting fluid displacement is not ideally symmetric. We leverage this observation to quantify the degree of variability. For this we quantify asymmetry by measuring the Wasserstein distance of the regularized experimental data sets and its mirrored image, across the presumed North-South symmetry plane (along the fracture). The resulting symmetry error for the experiments with symmetric characteristics is shown in **Figure 8Sb**. Consistent with the main text, we use relative distances based on the reference value defined by one of the two regularized concentrations for the regularization error. We conclude that the relative symmetry error is

approximately 0.046 ± 0.013, indicating a high quality of the data. Due to the identical operating conditions, it is assumed that the symmetry error is also representative for the experimental data for Core C.

REFERENCES

1. Both, J. W., Facca, E., and Nordbotten, J. M. (2023). Iterative finite volume approximation of the 1-Wasserstein distance. [Manuscript in preparation].
2. Santambrogio, F. (2015). *Optimal Transport for Applied Mathematicians*. Birkäuser, NY, 55(58-63):94.